

FLUX AND STABLE ISOTOPE FRACTIONATION OF CO₂ IN A MESIC PRAIRIE HEADWATER STREAM

Brock S. Norwood, Randy L. Stotler, Pamela L. Sullivan, Andrea E. Brookfield, G. L. Macpherson*

B. S. Norwood, bnorwood027@gmail.com, DHI Group, Inc., Denver CO. and Department of Geological Sciences, University of Kansas

R.L. Stotler, randy.stotler@uwaterloo.ca, Department of Earth and Environmental Sciences, University of Waterloo, ORCID: 0000-0001-9893-9259

P. L. Sullivan, College of Earth, Ocean and Atmospheric Science, Oregon State University, OR, USA, 97331; pamela.sullivan@oregonstate.edu; ORCID 0000-0001-8780-8501

A.E. Brookfield, andrea.brookfield@uwaterloo.ca, Department of Earth and Environmental Sciences, University of Waterloo, ORCID: 0000-0003-3739-0025

*corresponding author. G. L. Macpherson, glmac@ku.edu Department of Geological Sciences, University of Kansas, ORCID: 0000-0001-7461-2788

ABSTRACT

This study quantifies small-scale carbon dioxide (CO₂) efflux and estimates annual CO₂ emission from a headwater stream at the Konza Prairie Long-Term Ecological Research Site and Biological Station (Konza), in a terrain of horizontal, alternating limestones and shales. We characterized the CO₂ efflux and stable carbon isotopes (¹³C-CO₂) at point sources of groundwater discharge from small-scale karst features, identified by temperature, and downstream of those point sources, as well as in stream reaches without identifiable point sources.

CO₂ effluxes ranged from 2.2 to 214 g CO₂ m⁻² day⁻¹ (mean was 20.9 ± 41.4 g CO₂ m⁻² day⁻¹). Downstream of point groundwater discharge sources, CO₂ efflux decreased, over 2 meters, to 3% to 40% of the point-source flux, while ¹³C-CO₂ increased, ranging from -9.8 ‰ to -23.2 ‰ V-PDB (mean was -14.9 ‰ ± 4.2 ‰ V-PDB). The ¹³C-CO₂ increase was not strictly proportional to the CO₂ flux but related to the origin of vadose-zone CO₂ (C3 versus C4 vegetation). Over the study period, ~7.0 metric tons of CO₂ were emitted from the 1.1-km-long stream, comparable to other headwater streams. The high spatial and temporal variability of CO₂ efflux from this headwater stream informs those doing similar measurements and those working on upscaling stream data, that local variability should be assessed to make the best estimate of the impact of headwater stream CO₂ efflux on the global carbon cycle.

PLAIN LANGUAGE SUMMARY

CO₂ efflux from a headwater stream in a mid-continental prairie terrain underlain by alternating thin limestones and shales shows large spatial and temporal variability. Where point sources of groundwater discharge to the stream were located by thermal imaging (temperature differences), CO₂ flux, over a distance

of 2 meters, decreased by 3% to 40% of the flux at the point source. Stable carbon isotopes ($^{13}\text{C-CO}_2$) increased with decreasing flux at individual locations and times, but overall could not be correlated unambiguously with flux magnitude. Although the estimated annual CO_2 flux is within the range of fluxes measured elsewhere, the nearly two-fold difference in the annual flux calculated with and without high CO_2 -flux outliers demonstrates the importance of better characterizing headwater streams for estimations of global C balances.

KEY WORDS

CO_2 efflux

Headwater stream

Stable carbon isotopes

CO_2

Merokarst

HIGHLIGHTS

- 1) An intermittent stream in merokarst terrain emitted 4-7 tons of C in one year, but efflux was highly variable spatially and temporally.
- 2) CO_2 efflux was rapid: two meters downstream of the point of groundwater discharge flux was 3% to 40% of the point-source flux.
- 3) $^{13}\text{C-CO}_2$ correlated negatively with CO_2 fluxes except for two high-flux values, suggesting $^{13}\text{C-CO}_2$ is not a reliable indicator of CO_2 flux.

1 Introduction

Headwater stream emission of CO_2 is a significant part of the short-term carbon cycle (Battin et al., 2009; Cole et al., 2007, 2010; Nadeau and Rains, 2007; Alin et al. 2011; Butman and Raymond, 2011; Striegl et al. 2012; Dinsmore et al., 2013; Atkins et al., 2013; Hotchkiss et al., 2015; Marx et al., 2017). Headwater streams are complex environments, accounting for more than half of all stream lengths globally (Nadeau and Rains, 2007). Small-scale heterogeneity that is common in these systems makes it difficult to characterize and upscale CO_2 cycling.

Carbon flux from streams depends on terrestrial production and storage of CO_2 in soil and in shallow aquifers, and on the hydrogeologic pathways that connect them: groundwater discharge is the primary source of dissolved gasses in low-order streams (Hope et al., 2001; Deirmendjian et al., 2018; Doctor et al., 2008; Johnson et al., 2008; Sand-Jensen and Staehr, 2012; Crawford et al., 2014; Hotchkiss et al., 2015), and shallow aquifers, not deep groundwater, are the main contributors of CO_2 (Hotchkiss et al., 2015). Hotchkiss et al. (2015) estimated that over 70% of CO_2 stream flux is produced terrestrially, with the majority of

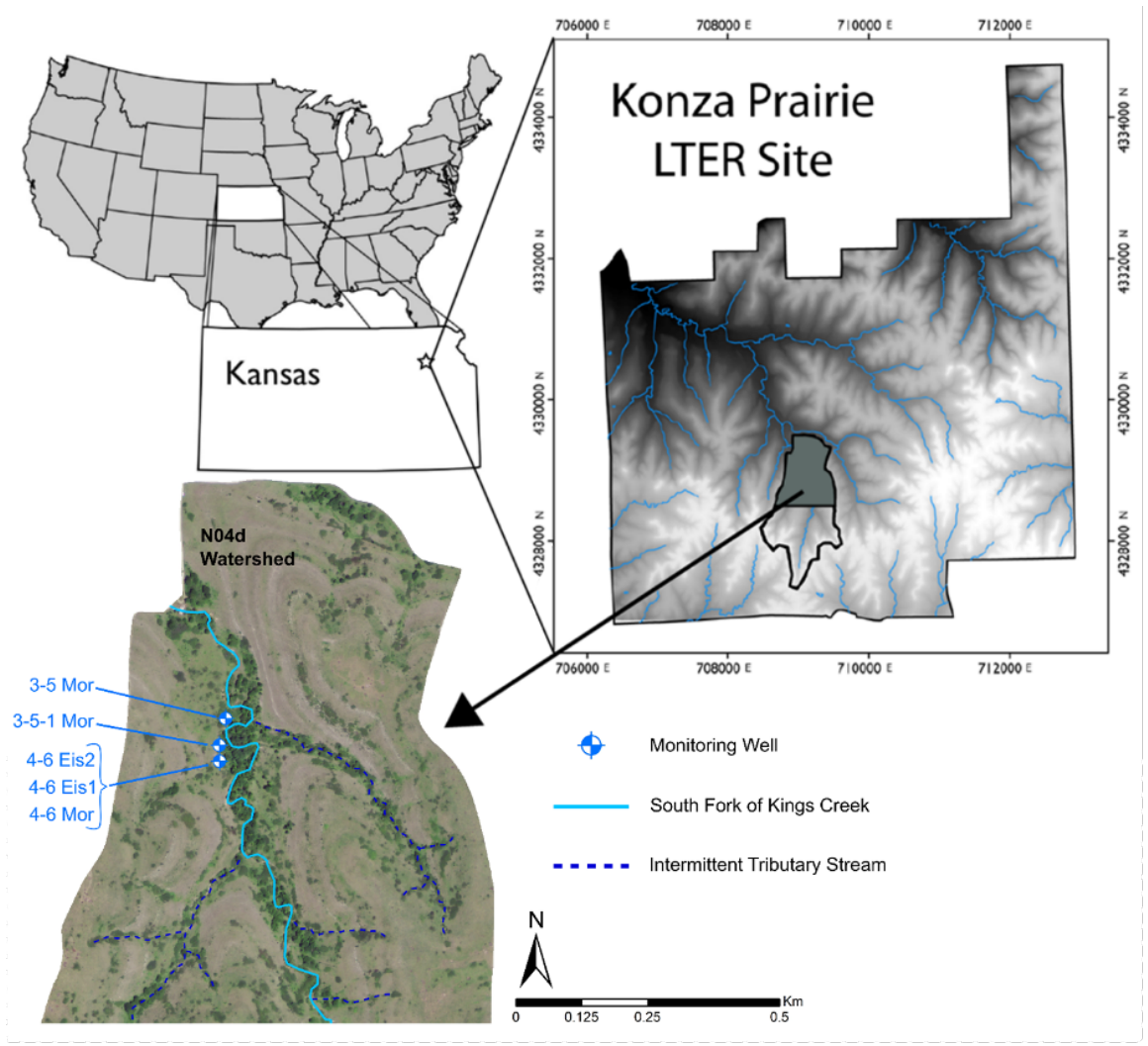
the terrestrial contribution derived from infiltration through soil; infiltrated water travels as interflow or as recharge to shallow groundwater that discharges to streams. Terrestrially-derived CO_2 is produced during organic matter degradation, and root and organism respiration. Meteoric water infiltrates soil, taking up soil CO_2 (Chapelle, 2000). Although most soil CO_2 escapes upward to the atmosphere, downward water migration dissolves and transports $\sim 1\text{-}2\%$ of soil CO_2 to groundwater (Hendry et al., 1993; Schlesinger and Lichter, 2001; Tsy-pin and Macpherson, 2012). Carbonic acid from dissolution of CO_2 dissolves carbonate minerals, releasing inorganic carbon into solution. These carbon fluxes lead to the accumulation of CO_2 in groundwater, with concentrations one to two orders of magnitude higher than in the atmosphere (Schlesinger and Melack, 1981; Macpherson et al., 2008; Macpherson 2009; Johnson et al., 2008; Monger et al., 2015; Macpherson and Sullivan, 2019). When groundwater discharges into surface water, gas efflux is driven by the concentration gradient between the water and atmosphere.

Given the extensive distribution of carbonate terrains across the world (Weary and Doctor, 2014; Chen et al., 2017) and the complexity of groundwater-surface water interactions, it is necessary to better quantify CO_2 efflux in carbonate-hosted headwaters and relate the CO_2 flux to groundwater discharge. We present the results of a $\sim 1\text{-year}$ study of a headwater stream at the Konza Prairie Long-Term Ecological Research Site (LTER) and Biological Station (Konza), where merokarst (thin limestones alternating with shales) presents the opportunity to characterize point sources of groundwater discharge (point sources) and resulting CO_2 efflux. We contrast the CO_2 fluxes from the stream water passing over outcrops or subcrops of limestone and shale, quantify the stream CO_2 emission within the lower half of the watershed (~ 1.1 km stream length), and test how efflux is related to $^{13}\text{C}\text{-CO}_2$.

2 Field Site and Methods

2.1 Location: Konza is one of the last remaining undisturbed, tallgrass prairies in North America. The 3,487-ha research area is located in the Flint Hills, near Manhattan, Kansas (Figure 1a). The Flint Hills, unlike other prairie environments, lack soils suitable for tilling, which has reduced anthropogenic stresses on the ecosystem. Konza is divided into 60 watersheds with different research treatments; Tsy-pin and Macpherson (2012) showed the study watershed, N04d (1.2 km^2), is on a major watershed divide and is surrounded by grazed land. Stream reaches in watershed N04d are intermittent except for a few small pools that are dry only during the most severe droughts (Figure 1a, b).

a)



b)

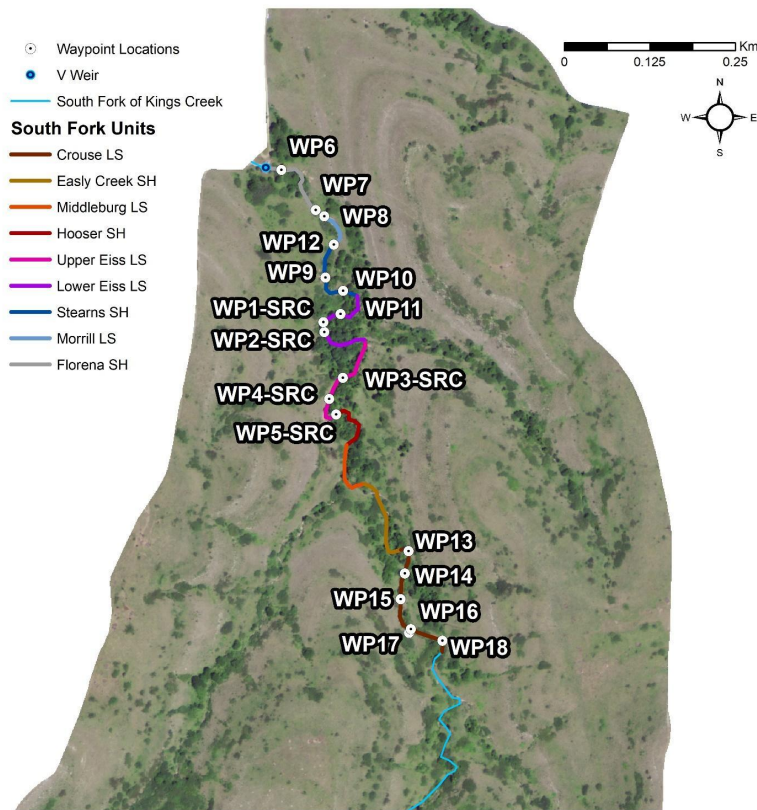


Figure 1. a) Location map of the Konza Prairie LTER Site with inset of the N04d watershed. Data from monitoring wells are included in Supplemental Information. b) Waypoint (WP) GPS locations and stream reach discretization based on geology along the South Fork of Kings Creek. SRC: point source location. MS (midstream) and DS (downstream) locations are 1 m and 2 m from SRC locations, so are not resolved on this scale map and are labeled with a single WP. Stream flows north. WP 17 is a spring ~5 m above the streambank.

2.2 Climate: Konza has a temperate, mid-continental climate (Hayden, 1998), with high variability both seasonally and annually (Nippert and Knapp, 2007). From 1983 to 2016 (Nippert, 2017), average daily air temperature at Konza was 12.8 °C and mean total annual precipitation was 839 mm. From July 2015 to August 2016, the period of this study, average air temperature was 14.9°C

and precipitation was 974 mm (116% of the annual mean precipitation; Table 1); 70% of precipitation fell during the growing season (March to October). On an annual basis, both 2015 and 2016 exceeded both the long-term average precipitation and air temperature.

Table 1: Climate and hydrology data

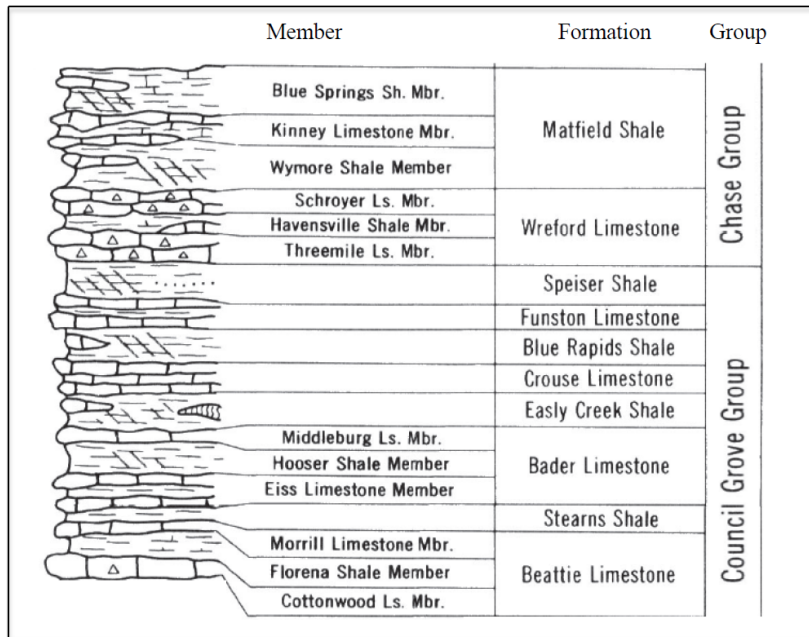
Climate and hydrology*	1983-2016	2015	2016	Study Period†
Average daily air temperature (°C)	12.8	13.7	14.4	14.9/14.3
% of long-term average (1985-2016)	100%	107%	112%	116%/112%
Total precipitation (mm)	839	1003	991	974/938
% of long-term average (1983-2016)		119%	118%	116%/114%
Mean discharge (m ³ d ⁻¹)		486	860	769/741
Median discharge (m ³ d ⁻¹)		0	186	138/133
Jan 1 to August sampling date, sum (m ³)		140,495	273,931	

* Data from CLIMDB/HYDRODB (2021).

† First number is the study period (379 days). Second number is converted to an annual value (365 days).

2.3 Vegetation: Konza lies along the southeastern margin of the North American Prairie (Hayden, 1998). Konza flora is dominated by C₄ grasses and forbs (C₃), while woody vegetation (C₃) is found in patches in riparian zones and on hillslopes (Veach et al., 2014). C₃ and C₄ plants differ in their method of carbon fixation during photosynthesis (Wang et al. 2012), which affects the ¹³C of CO₂ produced during breakdown of the plants.

2.4 Geology: Konza is underlain by thin soils and merokarst. The loess-based soils, primarily silty clays and silty clay loams (NRCS, 2006), are thickest (~1 meter) at the base of slopes and patchy on the plateaus (Ranson et al., 1998). The merokarst is thin, interlayered beds of Lower Permian age limestones (mostly 1-2m) and thicker shales (4-6m; Figure 2); discontinuous Quaternary alluvium occupies valleys. Bedrock strikes northeast-southwest and dips ~2° northwest (Twiss, 1988). Limestone outcrops form flat uplands and benches along the hillsides; slopes form over shales. Streams dissect the landscape into relatively steep-sided valleys (Macpherson, 1996). The limestones and alluvium act as aquifers and shales as aquitards; many of the limestones are hydraulically connected to the streams (Macpherson et al., 2008). Hydraulic conductivities of the limestones, controlled by secondary porosity, range over five orders of magnitude (10⁻⁸ to 10⁻³ m s⁻¹; Pomes, 1995; Sullivan et al., 2020).



Abbreviations: Ls.: limestone. Sh.: shale. Mbr.: member.

Figure 2: Stratigraphic column of the geology at Konza (modified, from Zeller, 1968).

2.5 Sampling: Geologic mapping, measurement sites, and sampling sites spanned 1125 m of the South Fork of Kings Creek (Figures 1b) and were located with a Garmin Etrex Legend GPS (Supplemental, Table S1). Stream segments were discretized, based on geology, into nine reaches (Figure 3). Those underlain by shale and limestone account for 41% and 59% of the total stream length, respectively. Stream reaches underlain by shale are narrower than reaches underlain by limestone; for calculation purposes, widths of stream reaches underlain by shale were set at 1.0 meter and those by limestones at 1.5 meters. For the sake of brevity, units will be identified with their simplified geologic name: Crouse, Upper Eiss, Lower Eiss, Stearns, Morrill, Florena.

2.5.1 Suspended Chamber

CO₂ efflux from the stream was measured with a suspended chamber (Crawford et al., 2014; Rawitch et al., 2019). Two chamber designs were lab tested (Norwood, 2020) and used in the field. The first is a 3D-printed ABS plastic rectangular prism with rounded, triangular prisms on the front and back for streamlining; it has a small footprint ($9.40 \times 10^{-3} \text{ m}^2$) and was sealed with acetone vapor. The second is made with 5-mm thick plexiglass, is heavier, has the shape of a rectangular prism, and has a larger footprint ($1.55 \times 10^{-2} \text{ m}^2$).

For each trial, the bottom of the chamber was submerged ~2 cm below the

water surface. The chamber was connected to a pump and a Li-Cor LI-820 CO₂ Infrared Gas Analyzer (IRGA) using Tygon® tubing; the circulating air (1 L/min) passed through a Drierite® filter to remove moisture. CO₂ concentrations from the chamber were logged at one-second intervals; pressure changes in the chamber were minimized by returning analyzed gas to the chamber. Chamber trials lasted at least five minutes. Between trials, the chamber atmosphere was allowed to equilibrate with the atmosphere. Atmospheric CO₂ (ppm), temperature (°C), and relative humidity (RH, %) were measured using an AZ-77535 CO₂/Temperature/RH meter.

2.5.2 Sampling

Water and gas samples were collected over the 379 days between 21 July 2015 and 2 August 2016 (Supplemental Table S1). Gas samples were collected directly from the suspended chamber and stored in 0.5 L Tedlar® Gas-Sampling Bags for C isotope determination. Chemistry of groundwater and stream water were used to calculate aqueous $p\text{CO}_2$, using chemical analysis of water (inorganic species and pH; Supplemental Table S2, S3; Norwood, 2020) and then speciated with PHREEQC Interactive 3.1.7-9213 (Charlton, et al., 1997). Charge balances, also calculated by PHREEQC, are less than 5% for all but three analyses. Water chemistry is typical of limestone terrains, dominated by calcium and bicarbonate with slightly alkaline pH and moderate total dissolved solids. Analytical methods and results are similar to other studies done at the site (e.g., Macpherson, 1996; Macpherson et al., 2008; Macpherson and Sullivan, 2019).

2.5.3 Gas Stable Isotopes

A Picarro® G2201-I Analyzer for Isotopic CO₂/CH₄ was used to determine ¹³C-CO₂. Two reference standards for carbon dioxide gas (¹³C of -40.78‰ and -10.42‰, V-PDB) were used along with CO₂ gas standards (500 ppm and 1000 ppm) for calibration. Samples were injected directly into the Picarro analyzer from the gas-sampling bags. Between analyses, nitrogen gas flushed the Picarro of CO₂.

2.5.4 Stream discharge at Suspended Chamber Sites

Stream discharge was measured at nine WP locations on two different days using a ~30 cm long, 0.25 cm inside-diameter pitot tube. Streamflow measurements follow protocols outlined by the Environmental Protection Agency (Meals and Dressing, 2008) and the United States Geological Society (USGS, 2016).

2.5.5 Flux Calculations

Chamber flux (F_c) was calculated for each suspended chamber measurement as follows:

$$F_c = \left(\frac{d(\text{CO}_2)}{dt} \right) \left(\frac{p * V_c}{R * T * A_c} \right) \quad (1)$$

where $\left(\frac{d(\text{CO}_2)}{dt} \right)$ is the change in chamber CO_2 concentration with time, p is the gas pressure in the chamber, V_c is the chamber volume; R is the universal gas constant; T is the air temperature in Kelvin, and A_c is the surface area of water covered by the chamber (Müller et al., 2015). To determine $\left(\frac{d(\text{CO}_2)}{dt} \right)$, a linear regression was fit to the linear portion of the flux data; data were excluded if $R^2 < 0.90$. The diffusive transfer of gasses between a water surface and the atmosphere (F ; [$\text{ML}^{-3}\text{T}^{-1}$]) is:

$$F = k(C_w - C_{\text{atm}}) \quad (2)$$

where C_{atm} is the atmospheric gas concentration above the water body, C_w is the gas concentration in the water, and k is the gas transfer coefficient (MacIntyre et al., 1995). The gas transfer coefficient (gas transfer velocity) is temperature- and density-dependent (Demars and Manson, 2013; Wanninkhof, 2014). k is converted to k_{600} (Cole and Caraco 1998) to compare with other gas transfer rates at 20 °C.

To estimate the flux from the stream, we first calculated total daily flux (F_{TD}) ($\text{g CO}_2 \text{ day}^{-1}$) using average flux for each stream reach as follows:

$$F_{\text{TD}} = \sum (F_{\text{SU}} * A_{\text{SU}}) \quad (3)$$

F_{SU} is the daily flux ($\text{g CO}_2 \text{ m}^{-2} \text{ day}^{-1}$) and A_{SU} is the surface area (m^2) for each stream reach. For six of the stream reaches, average CO_2 flux was calculated using direct measurements. For two of the units where direct measurements were not made, mean CO_2 flux ($\text{mol m}^2 \text{ day}^{-1}$) was used for each rock type (shale or limestone). Mean CO_2 flux was also used for the Florena, as only one measurement was taken in that unit. Total flux for the study period (F_{SP}) was then determined by:

$$F_{\text{SP}} = F_{\text{TD}} * t \quad (4)$$

where t is days of recorded stream discharge at the triangle-throated flume (weir) at the northwestern end of the watershed (Figure 3).

3 Results

3.1 Stream discharge

The Konza LTER Program records stream discharge at the weir every five minutes; data are transformed to daily averages (Dodds, 2021). The discharge measurements at the weir are assumed to be a reliable indicator of upstream flow in N04d; however, we recorded discharge at upstream reaches on two dates when there was no flow at the weir. Over the study period, discharge was recorded at the weir 68% of the time (Figure 3). Mean discharge was $138 \text{ m}^3/\text{day}$; median discharge $402 \text{ m}^3/\text{day}$. The mean discharge and sum of daily discharge from 1 January 2016 to 2 August 2016 were almost twice as high as in 2015 (Table 1).

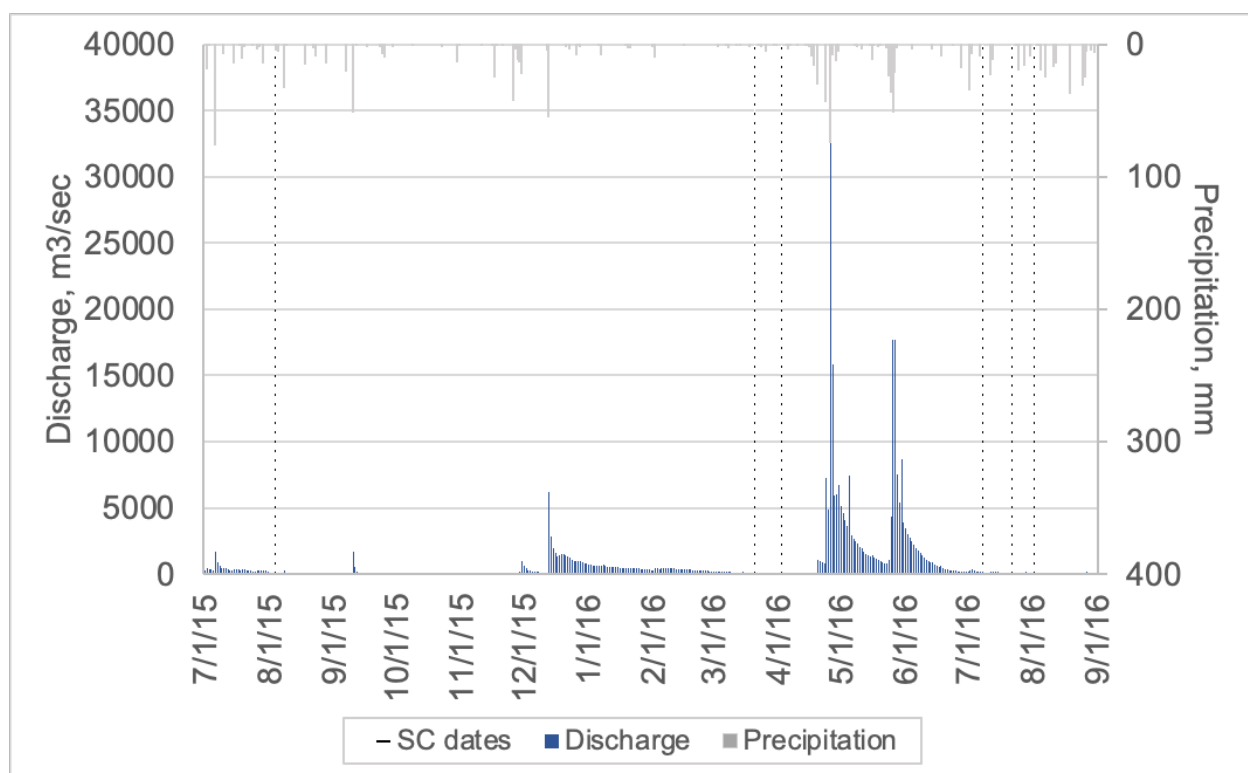


Figure 3: Stream discharge at the N04d weir in blue, dates of suspended chamber (SC) measurements as vertical dashed lines, and daily precipitation, in reverse order, on right axis in grey. (Precipitation: CLIMEDB/HYDRODB, 2021; discharge: Dodds, 2021).

Chamber-site discharge measurements made with the pitot tube varied over an order of magnitude; measurement points were ~ 50 to ~ 100 m apart (Figure 4). The upstream-most reach is underlain by the Crouse. Most other locations are also underlain by limestone, except WP-10B (Stearns). Note that no discharge was recorded at the weir on either of those days, illustrating that this is a losing

stream.

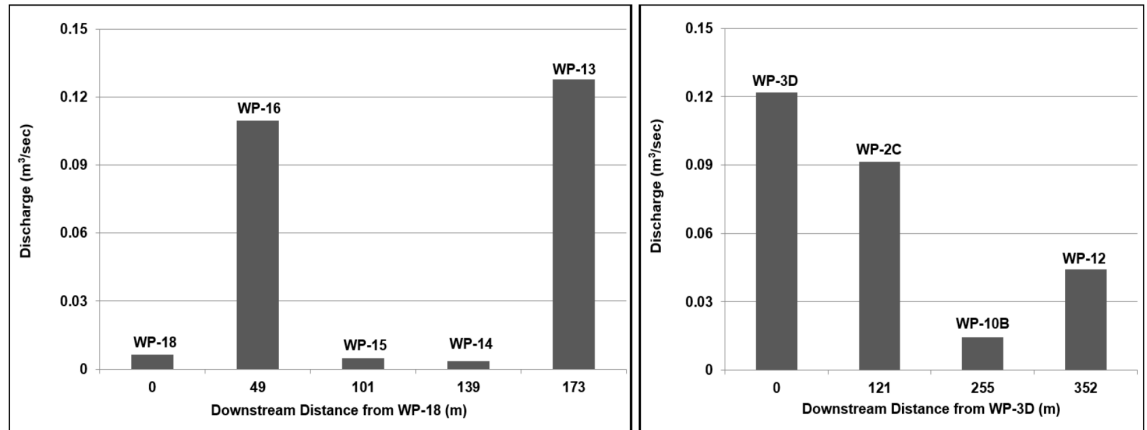


Figure 4: Stream discharge from upstream (left, Crouse, 2 August 2016) and downstream (right, Upper Eiss, Lower Eiss, Stearns, and Morrill, 22 July 2016).

3.2 Point discharge sources

Throughout most of the year, temperature differences exist between groundwater (Macpherson, 2020) and surface water (Nippert, 2017; Nippert and Knapp, 2017; Brookfield et al., 2017) at Konza. Average groundwater temperature was $\sim 16^{\circ}\text{C}$ for the study period, with average surface-water temperature $\sim 21^{\circ}\text{C}$. This temperature differential permitted location of point-source groundwater discharge locations (point sources) by a FLIR® T600 Thermal Imaging Infrared Camera (FLIR Camera). Seeps and springs flowing from fractures along the streambank and streambed were observed where underlain by the Morrill, Eiss (Figure 5), and Crouse limestones. These point sources were used to evaluate degassing lengths.

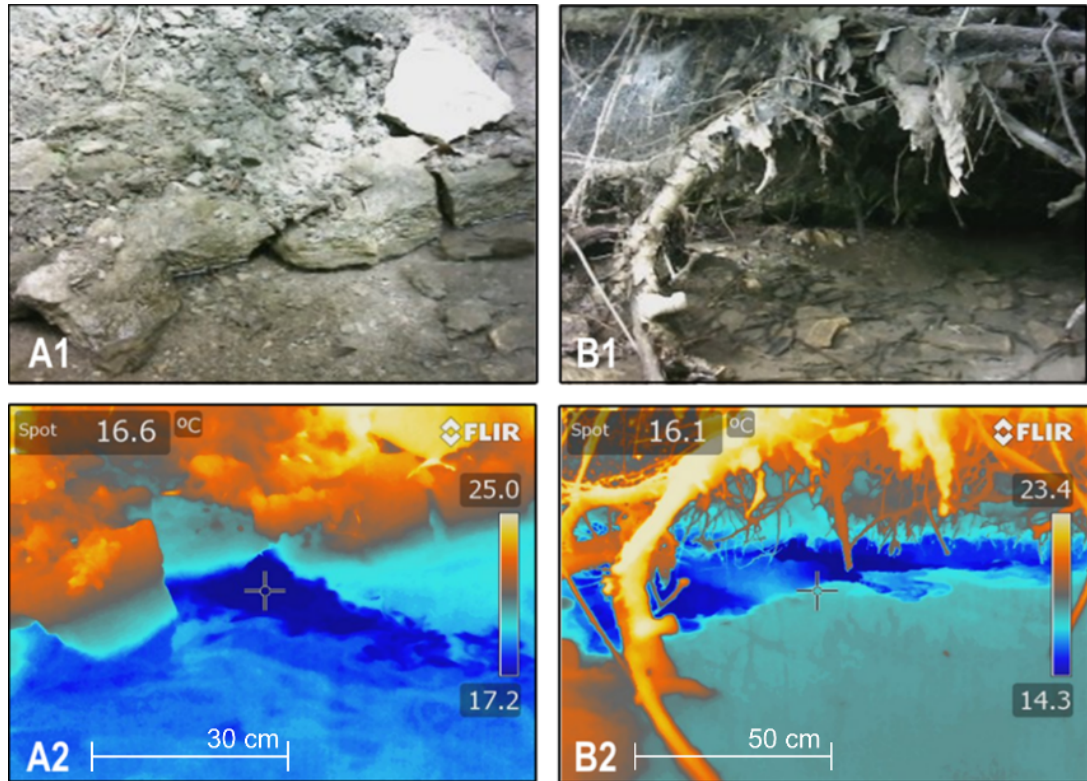


Figure 5: Infrared images of groundwater discharging from the Upper (A) and Lower (B) parts of the Eiss Limestone member into the South Fork. Standard digital black-and-white images (A1 and B1) and infrared images (A2 and B2) where blue colors are colder; orange colors, warmer.

3.3 Carbon Flux

Carbon flux measurements from the South Fork ranged from 2.2 to 214 g CO₂ m⁻² day⁻¹, with a mean CO₂ flux of 20.9 g CO₂ m⁻² day⁻¹ ± 41.4 g CO₂ m⁻² day⁻¹ (1 S.D.; Supplemental Table S1). WP-3A-SRC and WP-17 are high-flux outliers. For nearly all locations, flux measurements were higher for stream reaches underlain by limestone than those underlain by shale. The CO₂ fluxes measured in the three limestone units also varied, even between the more permeable (Upper Eiss) and less permeable (Lower Eiss) portions of the same limestone member (Table 2 and Supplemental Table S1). During the study period, the variability within a geologic unit, measured two to four times, was higher in high permeability units (Upper Eiss; Crouse [presumed high because of frequency of springs in this unit; Barry, 2018]) than low permeability units (Lower Eiss, Stearns, Morrill). Among the limestones, the CO₂ fluxes and the coefficients of variation of the CO₂ fluxes decreased with unit thickness (Table 2). Point sources were not found in stream reaches underlain by shale.

Table 2: Variability in measurements taken at same locations but different times

All with multiple measurements:

Measurement location	*	Mean	1 standard deviation	Coefficient of variation %	Count
Crouse Ls, WP-13		14.2	13.4	95%	2
Upper Eiss Ls, WP-4	SRC	14.1	16.3	116%	2
Upper Eiss Ls, WP-3	SRC	57.1	88.4	155%	5
	MS	35.8	18.5	52%	3
	DS	17.6	10.5	59%	3
Lower Eiss Ls, WP-2	SRC	13.1	4.6	35%	2
	MS	10.1	4.8	47%	2
	DS	7.3	1.4	19%	3
Lower Eiss Ls, WP-1	SRC	11.2	1.5	14%	2
	MS	13.7	0.2	1%	2
	DS	14.5	7.6	53%	2
Morrill Ls, WP-7		4.3	0.5	11%	2

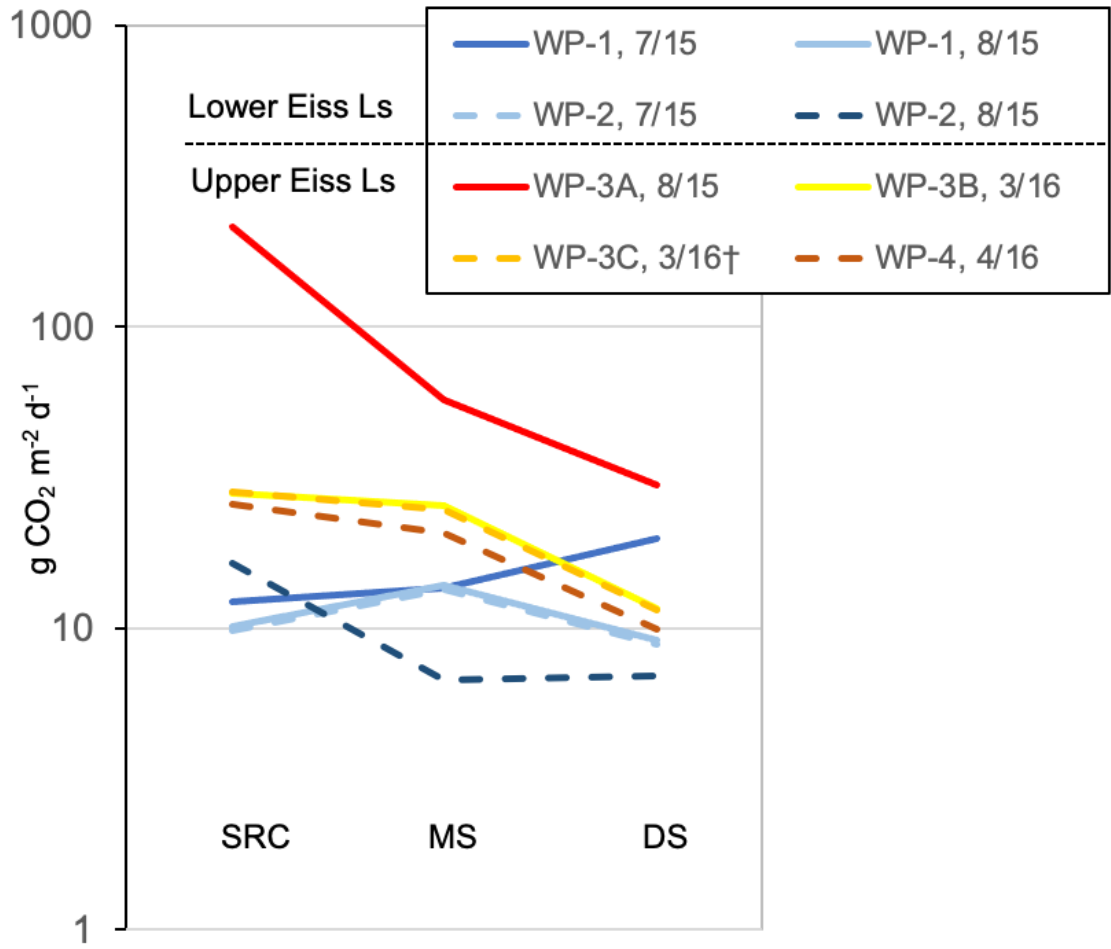
Without outliers:

Upper Eiss Ls, WP-3	SRC	17.8	12.1	68%	4
	MS	25.1	0.5	2%	2
	DS	11.6	0.1	1%	2

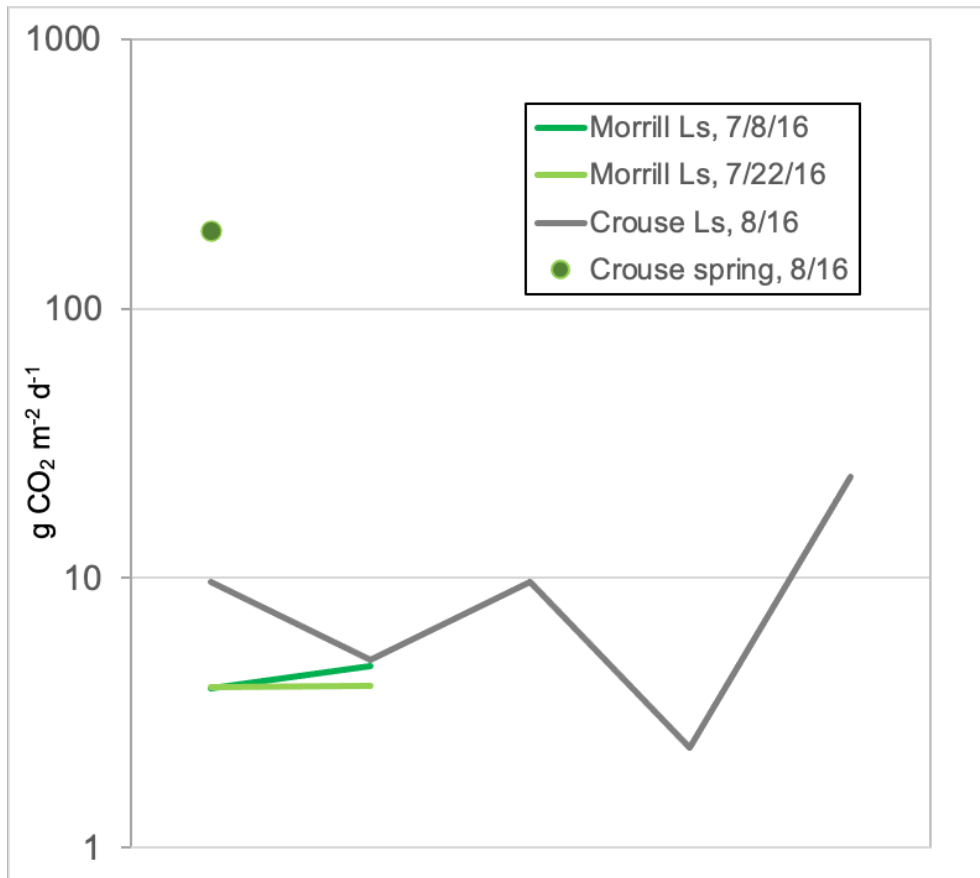
*SRC: point source of groundwater discharge; MS: midstream (1 m downstream of SRC); DS downstream (2 m downstream of SRC)

To investigate degassing lengths, measurements were made at the point source, 1 meter downstream, and 2 meters downstream. In the Upper Eiss reach, carbon flux at 2 meters downstream from the point source ranged from 14% to 42% of the point-source flux, decreasing in all trials (Figure 6a). Location WP-1 (Lower Eiss) had multiple rather than a single point source within the two-meter distance, resulting in non-uniform downstream fluxes. In the Upper Eiss reach, CO₂ flux ranged from ~7 to 214 g CO₂ m⁻² day⁻¹, the high value being an outlier; the Crouse spring located just west of the stream was the other high-flux outlier (Figure 6b). Figure 6a shows the trials where the groundwater discharge was measured directly, without influence of streamwater. This was accomplished using a half-pipe made of aluminum flashing and plastic sheeting to isolate the point-source water (location WP3, measured twice on the same day) and when there was no upstream flow (WP4). The WP-3 and WP-4 fluxes were similar, suggesting the isolation method was successful. The data in the lower hydraulic-conductivity Morrill reach and the long Crouse reach (Figure 6b) display irregular degassing patterns similar to the Lower Eiss reach.

a)



b)



c)

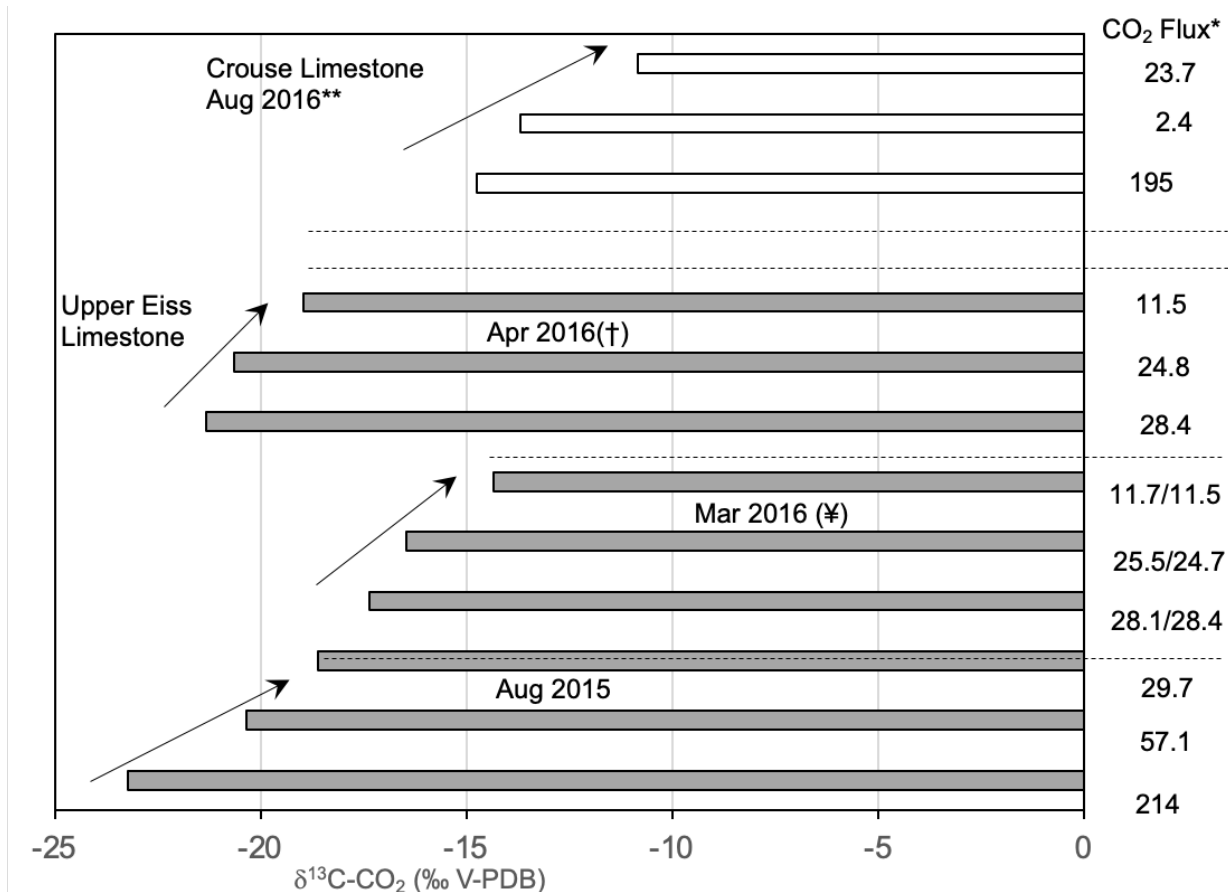


Figure 6: a) CO₂ flux changes over 2 meters. SRC: point source, MS: mid-stream, DS: downstream. b) Changes in fluxes within geologic units over longer distances (not to scale), including flux from a spring located about 5 meters west of the stream, which water feeds into the stream. c) Changes in ¹³C-CO₂ and flux with distance from point sources in Eiss and Crouse limestones. In each set of three, measurements are at point source and two locations downstream from the point source; arrows point in downstream direction. Crouse Limestone is the thicker of the two limestones represented here and is upstream of the Upper Eiss. The August 2015 and March 2016 data sets for the Upper Eiss Limestone are the same locations; the April 2016 location is ~50 m upstream.

* Flux units on left side of chart: g CO₂ per square meter per day.

** No GWCD, distance between collection points were ~80 m and 40 m.

† No upstream flow, so no GWCD; samples collected over 2 meters.

¥ Flux values, where paired, are with and without GWCD; isotope

samples from GWCD; samples collected over 2 meters.

Table 3 presents the mean CO₂ flux for each geologically-constrained stream reach during the 379-day study period. The average flux for all units was of the same order of magnitude with or without outliers: 14.5 ± 14.8 g CO₂ m⁻² day⁻¹ with and 10.2 ± 10.6 g CO₂ m⁻² day⁻¹ without outliers. Therefore, during the approximately 1-year study period, the South Fork emitted between 4.2 and 7.0 metric tons of CO₂ from the stream to the atmosphere.

Table 3: CO₂ properties of stream reaches underlain by geologic units.

Stream Segment*	Mean k600 (m/s)	Mean Flux (g CO ₂ /m ² /day)
Crouse LS	5.81E-08	35.7/9.18
Easley Creek SH‡	1.08E-08	3.48
Middleburg LS‡	2.55E-08	34.61
Hooser SH‡	1.08E-08	3.48
Upper Eiss LS	1.81E-08	31.7/19.5
Lower Eiss LS	7.07E-09	10.8
Stearns SH‡	1.13E-08	4.46
Morrill LS	2.22E-08	4.15
Florena SH	1.08E-08	2.51
Total stream length (m) and stream area (m²)		

* LS, Limestone; SH, Shale; informal names. See Figure 2 for full stratigraphic names.

† Where two values are entered, the first includes high flux outliers and the second excludes them.

‡ See text for how CO₂ flux was estimated where not measured.

3.4 Stable Carbon Isotopes

Stable carbon isotope ratios of chamber CO₂ (¹³C-CO₂) ranged from -9.7 ‰ to -23.2 ‰ (V-PDB) with a mean of -14.9 ± 4.2 ‰ (V-PDB) (Table S1). Gas samples collected at point sources have lower isotopic compositions (mean, -16.8 ± 3.0 ‰ V-PDB) than stream reaches with minimal groundwater influence (mean, -10.5 ± 0.4 ‰ V-PDB). Similar to CO₂ flux, small-scale spatial trends in ¹³C-CO₂ showed a consistent depletion in ¹²C from point source to downstream (Figure 6c).

4 Discussion

4.1 Spatial and Temporal Variability of CO₂ Flux

The spatially and temporally variable CO₂ fluxes and carbon isotopes in this study reflect the geomorphologic and hydrologic heterogeneity of the South Fork,

variable annual weather patterns, and vegetation. Point sources were only identified in reaches underlain by limestone and at geologic contacts between limestones and shales.

The spatial distribution of CO₂ flux along the South Fork is attributed to point sources of groundwater discharge. In addition, the highest daily CO₂ emissions corresponded to the thickest (Crouse) and most permeable (Upper Eiss) limestones (Figure 6a, b). Where 2-m measurements were made, most locations showed large decline in CO₂ efflux (Figure 6a, b), reinforcing the complexity of characterizing the contribution of degassed CO₂. In some stream reaches, multiple point sources occur over short distances, so degassing is more complicated than a simple decline (e.g., WP-1, Lower Eiss). In the Morrill reach (Figure 6b), the discharge and degassing patterns may also be complicated by the apparent upstream direction of groundwater flow in the subsurface, which then discharges below the weir, suggesting losing-stream behavior (Sullivan et al., 2020, their supplemental information; Barry, 2018); and small-scale gaining and losing stream behavior within the outcrop in the stream (Norwood, 2020). The long outcrop of the Crouse in the upstream portion (Figure 1b, Table 3) had multiple point sources with different CO₂ fluxes (Figure 6b): the highest and second highest CO₂ fluxes there correspond to a spring located just west of the stream and to the Crouse Limestone-Easley Creek Shale boundary, suggesting the importance of less permeable units forcing groundwater discharge.

The rate at which CO₂ efflux decreases downstream of point sources depends mostly upon the initial flux rate at the point source location. For example, when CO₂ flux at the point source exceeded ~195 g CO₂ m⁻² day⁻¹ (the two outlier locations), flux rates 2 meters downstream decreased to ~3-14% of the point source flux. However, when point source CO₂ flux was less than 195 g CO₂ m⁻² day⁻¹, the decrease at 2 meters downstream was ~40% of the point source CO₂ flux. The lowest flux measured at a point source in the two-meter spatial distribution trials was from the Lower Eiss (WP-2B, Table 2) at 16.4 g CO₂ m⁻² day⁻¹. Even at this low initial CO₂ flux, the flux two meters downstream of the point source decreased to ~40% of the initial flux (6.9 g CO₂ m⁻² day⁻¹). Based on the spatial distribution of carbon flux rates at point discharge sources, we conclude the majority of stream CO₂ degasses within the first 2 meters of entering the stream.

Repeat measurements at the same locations demonstrate the variability in CO₂ flux at this site (Figure 6, Table 3). Others have documented stream CO₂ content that may be strongly influenced by diurnal, seasonal, and annual factors (e.g., Hotchkiss et al., 2015). We propose that flux variability results from variations in hydraulic conductivity, as well as weather-driven recharge and groundwater flow directions. Table 3 shows the variability in measurements for all locations where at least two measurements were made. For measurements in limestones with lower hydraulic conductivity (Morrill, Lower Eiss), coefficients of variation of CO₂ flux are lower (1% to 53%) than those for limestones with higher hydraulic conductivity (Upper Eiss, Crouse; 52% to 155%).

The inverse relation between annual stream discharge and CO₂ efflux (Figure 7) suggests a link to watershed recharge dynamics, with less recharge allowing buildup of soil and/or groundwater CO₂ and subsequent discharge to the stream resulting in higher CO₂ efflux. The variation in groundwater CO₂ (Macpherson et al., 2008), where highest CO₂ occurs from September to November and lowest in February to April, is not reflected in the stream CO₂ flux data we collected. A systematic investigation of temporal trends in stream CO₂ flux seems necessary to relate seasonal groundwater CO₂ levels to flux data at point sources along the stream. Note that because the aquifers at this site are limestones, the stream can be gaining or losing depending on recent recharge: at high stream stage, the degassed stream water will enter the aquifer at the point sources and then later discharge at the same locations at low stream stage (e.g., Pomes, 1995; Macpherson and Sophocleous, 2004), further complicating interpretation of CO₂ flux dynamics. This phenomenon is likely not unique to karst systems, but possible whenever there are large changes in stream stage (Winter et al., 1998).

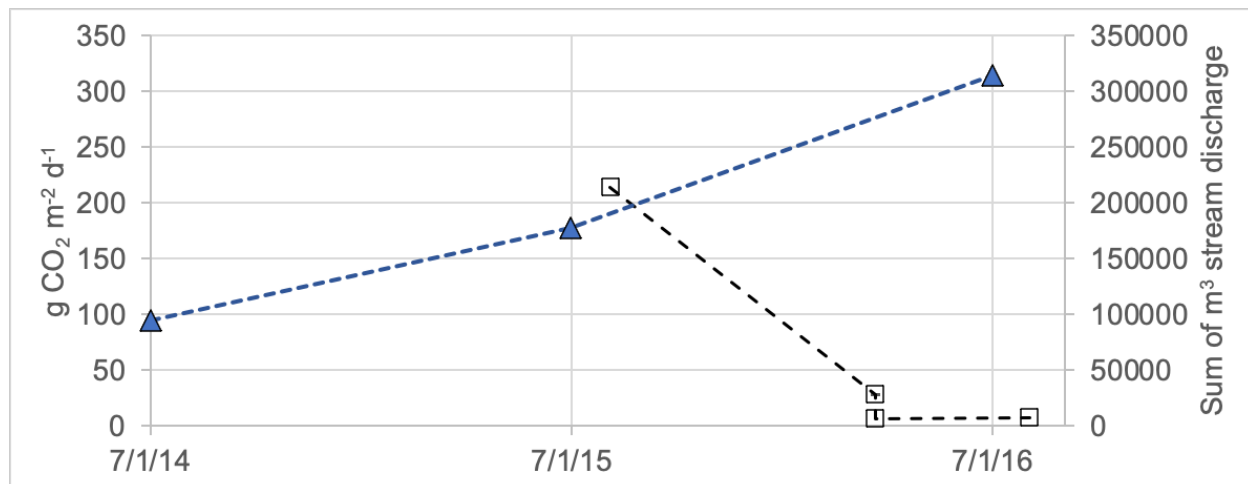


Figure 7: Sum of annual stream discharge (filled triangles, plotted at mid-year dates) and CO₂ flux (open squares) measured multiple times at one location (WP-3) on the stream. The higher March 2016 flux represents the average of 2 measurements taken on a single day; coefficient of variation for that data set is 3% which is smaller than the symbol size.

The k_{600} values ranged over two orders of magnitude, from ~ 0.0002 to ~ 0.02 m d⁻¹ (Supplemental Table S1). Excluding the highest k_{600} , which was measured at the Crouse spring (WP-17), the range lowers to one order of magnitude, (~ 0.0002 to ~ 0.008), within the range of other k_{600} 's measured in other headwater streams with low stream velocities (e.g., Rawitch et al., 2021).

4.2 Spatial and Temporal Variability of $^{13}\text{C-CO}_2$

During the two-meter trials, most gas samples showed an inverse relationship between $^{13}\text{C-CO}_2$ and CO_2 flux (Figure 6c, 7). Over the two-meter distance downstream of point sources, isotopic signatures are higher by $\sim 5\text{‰}$ to 7‰ (Figure 6c). Many have proposed that carbon isotope exchange with atmospheric CO_2 ($^{13}\text{C} \sim -8\text{‰}$) is partly responsible for increasing downstream ^{13}C values measured in streams and rivers (Taylor and Fox, 1996; Yang et al., 1996; Atek-wana and Krishnamurthy, 1998; Karim and Veizer, 2000; Helie et al., 2002; Mayorga et al., 2005). However, isotopic equilibrium between dissolved CO_2 and atmospheric CO_2 can only be attained after equilibrium of CO_2 concentration between atmosphere and stream/river water (Doctor et al., 2008). Thus, if a drive for CO_2 flux from water to the atmosphere exists, as observed in this study, fractionation of $^{13}\text{C-CO}_2$ will be primarily affected by gas efflux, rather than the carbon isotope exchange that accompanies carbon mixing. The observed depletion in ^{12}C during degassing therefore supports the hypothesis proposed by Doctor et al. (2008) and Venkiteswaran et al. (2014) that fractionation in the isotopic composition of DIC or CO_2 is driven by the process of gas transfer from stream to atmosphere, rather than mixing of CO_2 between the stream and atmosphere.

With two exceptions, CO_2 efflux rates show strong ($R = 0.60$ to 0.79) negative correlation with $^{13}\text{C-CO}_2$ (Figure 8; $R = -0.69$, $p < 0.0001$); the exceptions are two events with the highest flux rates. This lack of overall correlation indicates the flux rate is an unreliable predictor of $^{13}\text{C-CO}_2$. This contrasts with results from a sandy lowland watershed with more continuous groundwater discharge (Deirmendjian and Abril 2018).

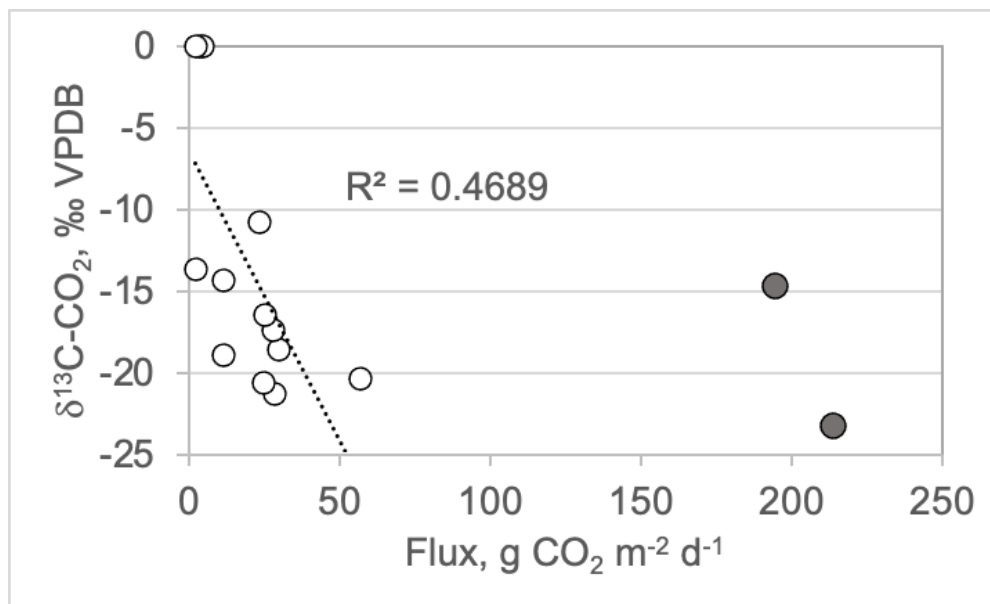


Figure 8: All but the two highest flux measurements show a significant, negative correlation with $^{13}\text{C-CO}_2$.

We propose that the $^{13}\text{C-CO}_2$ at point sources is controlled by processes other than flux rate. We suggest the controls include supply of CO_2 to groundwater from soil (e.g., Kessler and Harvey, 2001; Andrews and Schlesinger, 2001; Macpherson et al., 2008; Tsy-pin and Macpherson, 2012), vegetation type, variation in precipitation and streamflow, and degree of interaction with the limestone aquifers. The main sources of soil CO_2 are root respiration and microbial oxidation of organic C (Kuz'yakov and Domanski, 2000; Cisneros-Dozal et al. 2006; Wen et al., 2021). Thus, $^{13}\text{C-CO}_2$ in the soil atmosphere should reflect overlying vegetation. At this site, there are both C_3 plants (generally -27‰) and C_4 plants (generally -13‰); their isotope ratio is also affected by moisture content, temperature (Brown et al. 2009), recharge timing (Brookfield et al., 2017), and other factors related to vegetation functioning (e.g., Cernusak et al., 2013). The $^{13}\text{C-CO}_2$ in stream gas samples, for those closest to the point sources, should relate to groundwater $^{13}\text{C-DIC}$, groundwater travel distance (degree of reaction with the limestone), and nearby vegetation type assuming soil CO_2 continues to be added to groundwater as it approaches the stream (Figure 9). Enrichment in ^{13}C caused by dissolved CO_2 reacting with the marine limestone aquifer material will have the greatest effect on ^{13}C in the groundwater: (1) that has traveled longer distances, and (2) moves slower (low-hydraulic-conductivity units). At the study site, a mixture of woody plants and grasses are found above and near the Crouse Limestone, Stearns Shale, and Morrill Limestone reaches, while Eiss Limestone locations are located in a densely wooded riparian zone. The mean $^{13}\text{C-CO}_2$ values within 1-2 m of discharge locations in stream reaches underlain by the Eiss Limestone and the Crouse Limestone were $-21.0 \pm 2.3\text{‰}$ (V-PDB) and $-14.7 \pm 0.0 \text{‰}$ (V-PDB) respectively, reflecting the nearby vegetation (Figure 10).

The largest number of measurements in a single geologic unit, point sources in the Upper Eiss Limestone (Figure 10), demonstrate variable weather and climate. Moisture, as reflected by precipitation and streamflow, is a primary control, as it affects aquifer-to-stream or stream-to-aquifer travel directions, residence times (reaction times), and plant functioning. Further, at Konza the general direction of groundwater flow has been shown to be opposite of the streamflow direction in the Morrill but the same as streamflow in the Eiss (Sullivan et al., 2020, supplemental information). The variation in CO_2 flux and isotopic values measured in the Eiss further illustrate the complexity of characterizing CO_2 flux in headwater streams with: 1) thin limestone aquifers, with and without point sources; 2) large interannual variations in total meteoric precipitation and in timing of meteoric precipitation; and 3) large interannual variations in stream discharge.

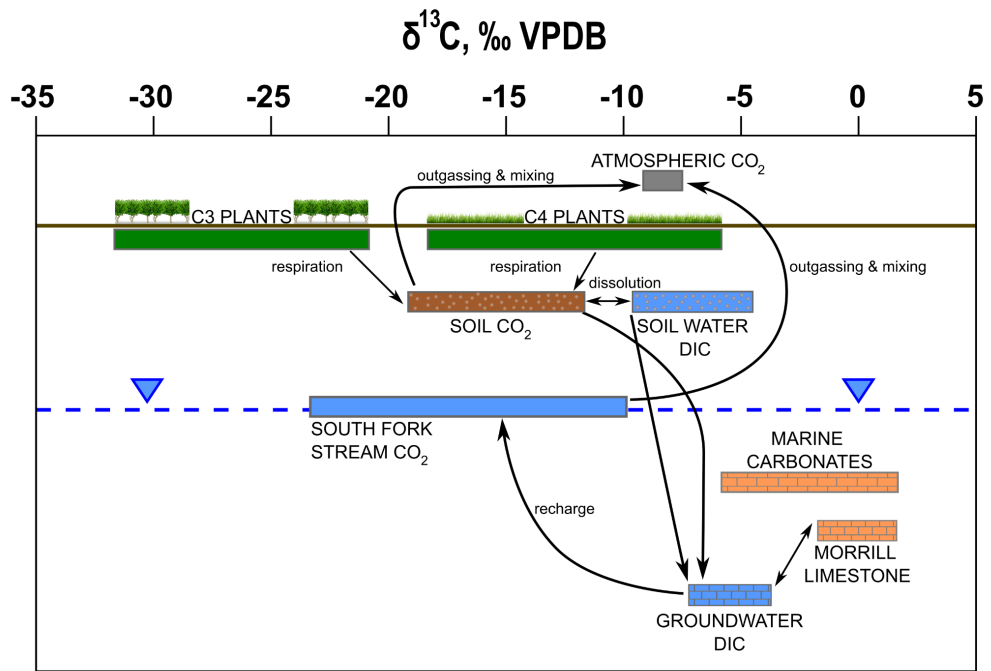


Figure 9: Representation of stable carbon isotope ranges for carbon reservoirs at the study site.

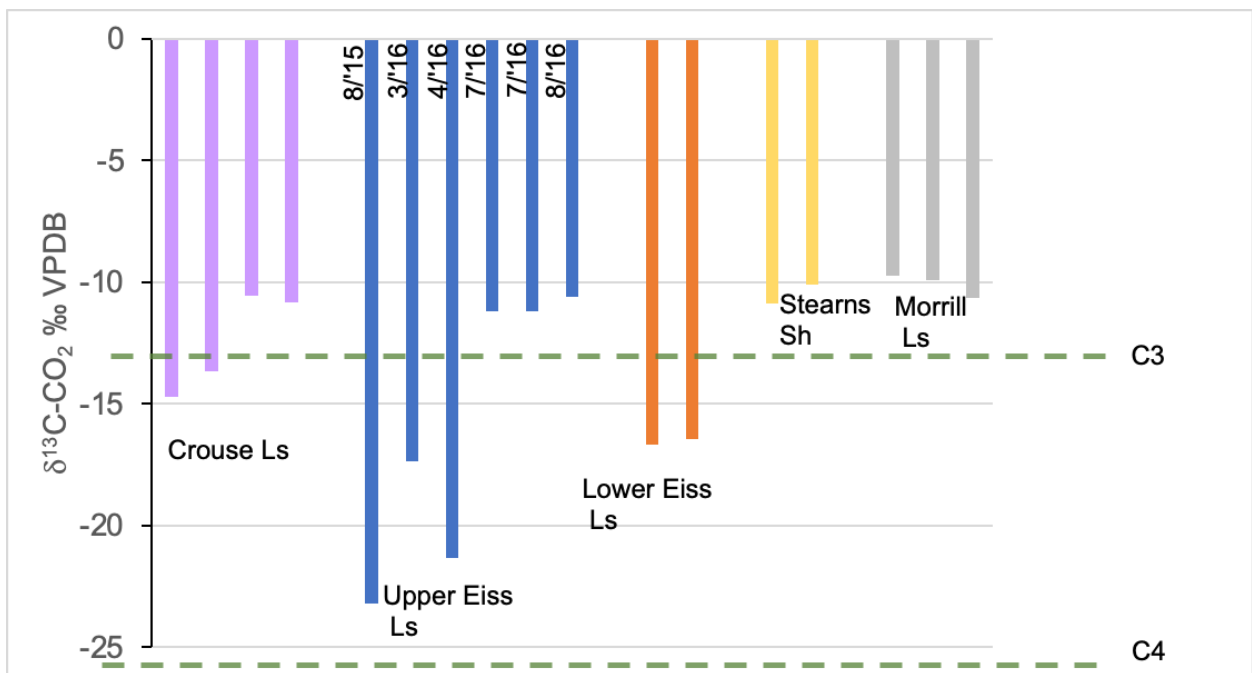


Figure 10: Carbon isotope ratios of CO₂ efflux from stream water. Point sources are plotted for Upper Eiss (sampling month and year indicated) and Lower Eiss; stream reaches with no identified point sources include Stearns and Morrill. The lightest Crouse value is from the spring which is just west of the stream; the other Crouse values are from downstream locations underlain by the Crouse.

The difference between CO₂ flux and ¹³C-CO₂ collected from the Upper Eiss in 2015 and 2016 and the Crouse in 2016 illustrates the effect of hydrologic response to meteorology (Table 1, 4), and limestone heterogeneity. In drier years, such as 2015 (preceded by an even drier year in 2014; Table 4, Supplemental Figure S1), groundwater residence time is longer and the build-up of CO₂ in groundwater is evidenced as higher CO₂ in point sources discharging to the stream. Higher water tables in wetter years reduce the distance between the surface and water table, with a wetter vadose zone increasing the unsaturated hydraulic conductivity, lowering groundwater residence time (Brookfield et al., 2017).

Table 4: Comparison of 2015 and 2016 selected field measurements and hydrology

Geologic Unit	Upper Eiss Limestone	Upper Eiss Limestone	Crouse Limestone
Waypoint	WP-3A-SRC	WP-3E-SRC	WP-17
Date measured	8/4/2015	8/2/2016	8/2/2016
CO ₂ flux (g CO ₂ m ⁻² day ⁻¹)	226	7.70	227
¹³ C-CO ₂ (‰ PDB)	-23.2	-10.6	-14.7
South Fork Discharge, (m ³ /year)			
2014	95,161		
2015	177,336		
2016	314,669		

4.3 Characterization of CO₂ Flux from the South Fork Watershed

Characterizing gas efflux from headwater streams is challenging because of small-scale spatial and temporal variability. Nevertheless, we propose that the data collected in this study approximate a characterization of CO₂ flux from the South Fork given the following assumptions:

- The stream width (m) and area (m²) for the nine stream reaches presented in Table 3 remain constant.
- The entire length of the South Fork (1125 m) flows on days when discharge is recorded at the weir. This could lead to an over prediction of total annual CO₂ flux. However, stream discharge was measured in multiple upstream reaches on days when no discharge was measured at the weir (Figure 4), so we will assume

these two issues offset each other.

- Suspended chamber measurements and gas samples collected for $^{13}\text{C-CO}_2$ are representative, although limited to spring and summer months, which could result in an over prediction of total annual CO_2 flux.
- Uncharacterized outgassing during dry periods (Catalán et al., 2014; Gomez-Gener et al., 2015; 2016), which could lead to an under-prediction of total annual CO_2 flux, are small..

Notwithstanding the potential limitations in flux calculations, during the study period, the South Fork emitted 7.0 metric tons of CO_2 when upper outliers were included, or 4.2 metric tons of CO_2 when excluded (Table 5). This CO_2 flux is intermediate to others reported in the literature (Table 5), an expected result considering the temperate climate. The actual total CO_2 flux from the stream surface could be closer to the lower value (4.2 metric tons of CO_2), given the limited stream surface area that was found to emit large amounts of CO_2 and the short period of streamflow during the growing season (Tsypin and Macpherson, 2012), which is when significant amounts of CO_2 are generated. However, calculating total flux from the stream surface including the high outliers may better reflect the true total flux, given some point sources could have been missed and considering we did not measure efflux in times of no streamflow. Given that the South Fork was dry for 32% of the study period, it is possible that annual CO_2 emission from the South Fork may exceed 7 metric tons even when excluding the upper outliers.

Table 5: Selected CO_2 flux rates from various stream environments.

Location	Environment	CO_2 Flux ($\text{g CO}_2 \text{ m}^{-2} \text{ d}^{-1}$)	Reference
Northern, Sweden	Boreal Streams		Jonsson et al., 2007
Yukon River Basin, USA	Rivers and Streams		Striegl et al., 2012
Mediterranean	Intermittent Fluvial Network		Gomez-Gener et al., 2015
Kansas, USA	Headwater Stream	*	This Study (No Outliers)
Zealand, Denmark	Upland Stream		Sand-Jensen and Staehr, 2012
Jinshui River Basin, China	River		Luo et al., 2019
Mediterranean	dry streambed		Gomez-Gener et al., 2016

Kansas, USA	Headwater Stream	†	This Study (Outliers Included)
France	First order streams		Deirmendjian and Abril, 2018
Alaska, USA	Boreal Streams		Crawford et al., 2013
Conterminous	Headwater Streams		Butman and Raymond, 2011
Colorado, USA	Subalpine		Clow et al., 2021
Banchory, UK	Headwater Stream		Hope et al., 2001

* equivalent to 4.2 metric tons per year

† equivalent to 7.0 metric tons per year

The high temporal and spatial variability of CO₂ efflux from this 1.1 km portion of a headwater stream makes it challenging to upscale the annual flux estimation. Recognizing the variability can inform others making efforts to scale-up river and stream CO₂ fluxes in order to gain a better understanding of the role of headwater and higher-order streams in the carbon cycle (e.g., Riveros-Iregui McGlynn, 2009; Ågren and Lidberg, 2019; Warner et al., 2019; Casio-Ruiz et al., 2021; Clow et al., 2021; Karlsson et al., 2021; Reitz et al., 2021; Saccardi and Winnick, 2021).

5 Conclusions

This study examines the timing and extent of CO₂ transport from shallow aquifers to the atmosphere and supports findings from similar studies that headwater streams are significant contributors in local and regional carbon cycling. At Konza, 45 measurements of CO₂ efflux were taken at 18 different locations along a headwater stream. The spatial variability of CO₂ flux along the 1.1-km stream segment reflects the underlying merokarst geology and the rapid decrease in CO₂ flux downstream of point sources of discharge. Point sources, detected by water temperature, were only observed in reaches underlain by limestones; at point sources, CO₂ flux measured two meters downstream from the point source ranged from 3% to 40% of the point source flux, regardless of the magnitude of the point-source CO₂ flux.

Over the ~1-year study period, we estimate 7.0 metric tons of CO₂ was emitted from the stream or 4.2 metric tons if the two high-end outliers are excluded. CO₂ efflux was not measured when the stream was dry, and considering the stream did not flow for 32% of the study period, the true annual flux could be higher.

The stable isotopic composition of CO₂ (¹³C-CO₂) was studied as a potential tracer of groundwater influx and predictor of CO₂ efflux rate. Lower ¹³C-CO₂ values were often accompanied by larger CO₂ fluxes, but the inverse relationship is not predictive, likely because disequilibrium between stream CO₂ and atmospheric CO₂ is the main driver of efflux. Thus, ¹³C-CO₂ can be a reliable indicator of groundwater discharge into a stream where a high contrast in partial pressure of CO₂ exists between groundwater and streamwater, but it is not a reliable indicator of CO₂ efflux rate.

The large range of CO₂ fluxes and ¹³C-CO₂ values observed over small spatial extents reinforces the importance of point-source measurements in headwater streams, especially in those areas where karst, or other preferential flow paths, controls groundwater flow. For this reason, large-scale investigations of stream degassing based on tracer tests or mass balance equations may overlook significant CO₂ contributions. The suspended chamber proved to be a simple and effective method for collecting measurements of CO₂ flux directly from the stream surface. This study provides additional reason to consider shallow aquifers and headwater streams when accounting for carbon sinks and sources on local, regional, and global scales.

Acknowledgements

Climate and stream discharge data sets were provided by the Climate and Hydrology Database Projects (<http://climhy.lternet.edu/>), a partnership between the Long-Term Ecological Research program and the U.S. Forest Service Pacific Northwest Research Station, Corvallis, Oregon. Significant funding for these data was provided by the National Science Foundation Long-Term Ecological Research program and the USDA Forest Service. BSN and GLM are grateful for support from the Konza Prairie LTER program (DEB-0823341 and DEB-1440484), the Geology Associates Fund of the KU Endowment Association, and the KU Department of Geology. A portion of coauthor PLS's time was supported by NSF EAR 2024388. BSN thanks Mike Rawitch, Trevor Osorno, Emily Barry, Mackenzie Creamens, and Brooks Bailey for field assistance and consultation.

References

- Ågren, A.M., Lidberg, W., 2019. The importance of better mapping of stream networks using high resolution digital elevation models—upscaling from watershed scale to regional and national scales. *Hydrology and Earth System Sciences Discussions*, pp.1-20.
- Alin, S.R., de Fátima, F.L., Rasera, M., Salimon, C.I., Richey, J.E., Holtgrieve, G.W., Krusche, A.V., Snidvongs, A., 2011. Physical controls on carbon dioxide transfer velocity and flux in low-gradient river systems and implications for regional carbon budgets. *Journal of Geophysical Research Biogeosciences*. <https://doi.org/10.1029/2010JG001398>

- Andrews, J. A., Schlesinger, W. H., 2001. Soil CO₂ dynamics, acidification, and chemical weathering in a temperate forest, with experimental CO₂ enrichment. *Global Biogeochemical Cycles*. 15, 149–162.
- Atekwana, E.A., Krishnamurthy, R.V., 1998. Seasonal variations of dissolved inorganic carbon and ¹³C of surface waters: application of a modified gas evolution technique. *Journal of Hydrology*, 205(3-4), pp.265-278.
- Atkins, M. L., Santos, I.R., Ruiz-Halpern, S., Maher, D. T., 2013. Carbon dioxide dynamics driven by groundwater discharge in a coastal floodplain creek. *Journal of Hydrology* 493: 30-42.
- Barry, E., 2018. Characterizing groundwater flow through merokarst, northeast Kansas, USA. U of Kansas unpublished M.S. thesis, Lawrence, KS, 118 pp.
- Battin, T.J., Kaplan, L.A., Findlay, S., Hopkinson, C.S., Marti, E., Packman, A.I, Newbold, J.D., Sabater, F., 2009. Erratum: Biophysical controls on organic carbon fluxes in fluvial networks.” *Nature Geoscience* 2.8: 59.
- Brookfield, A., Macpherson, G.L., Covington, M., 2017. Effects of changing meteoric precipitation patterns on groundwater temperature in karst environments. *Groundwater* 55.2: 227-236.
- Brown, T. L., LeMay, E. H., Bursten, B. E., Murphy, C. J., Woodward, P., 2009. Factors Affecting Solubility. *In* *Chemistry the Central Science* (11 ed., p. 541). Pearson.
- Butman, D., Raymond, P.A., 2011. Significant efflux of carbon dioxide from streams and rivers in the United States. *Nature Geoscience* 4.12: 839-42.
- Casio-Ruiz, J.P., Hutchins, R.H., del Giorgio, P.A., 2021. Total aquatic carbon emissions across the boreal biome of Québec driven by watershed slope. *Journal of Geophysical Research: Biogeosciences*, 126(1), p. e2020JG005863.
- Catalán, N., von Schiller, D., Marcé, R., Koschorreck, M., Gomez-Gener, L., Obrador, B., 2014. Carbon dioxide efflux during the flooding phase of temporary ponds. *Limnetica*, 33(2), pp.349-360.
- Cernusak, L.A., Ubierna, N., Winter, K., Holtum, J. A. M., Marshall, J. D., Farquhar, G. D., 2013. Environmental and physiological determinants of carbon isotope discrimination in terrestrial plants. *New Phytologist*, 200: 950–965. doi: 10.1111/nph.12423
- Chapelle, F. H., 2000. The significance of microbial processes in hydrogeology and geochemistry. *Hydrogeology Journal* 8.1: 41-46.

- Charlton, S. R., Macklin, C.L., Parkhurst, D. L., 1997. PHREEQCI, a Graphical User Interface for the Geochemical Computer Program PHREEQC. Lakewood, CO: U.S. Department of the Interior, U.S. Geological Survey, 1997.
- Chen, Z., Auler, A.S., Bakalowicz, M., Drew, D., Griger, F., Hartmann, J., Jiang, G., Moosdorf, N., Richts, A., Stevanovic, Z., Veni, G., 2017. The World Karst Aquifer Mapping project: concept, mapping procedure and map of Europe. *Hydrogeology Journal*, 25(3), pp.771-785.
- Cisneros-Dozal, L. M., Trumbore, S., Hanson, P. J., 2006. Partitioning sources of soil-respired CO₂ and their seasonal variation using a unique radiocarbon tracer." *Global Change Biology* 12.2: 194-204.
- CLIMEDB/HYDRODB (2021). <https://climhy.lternet.edu/>
- Clow, D.W., Striegl, R.G. & Dornblaser, M.M. (2021) Spatiotemporal dynamics of CO₂ gas exchange from headwater mountain streams. *Journal of Geophysical Research: Biogeosciences*, 126(9), p.e2021JG006509; <https://doi.org/10.1029/2021JG006509>.
- Cole, J. J., Caraco, N.F., 1998. Atmospheric exchange of carbon dioxide in a low-wind oligotrophic lake measured by the addition of SF₆. *Limnology and Oceanography* 43.4: 647-56.
- Cole, J. J., Bade, D. L., Bastviken, D., Pace, M. L., Van de Bogert, M., 2010. Multiple approaches to estimating air-water gas exchange in small lakes. *Limnology and Oceanography: Methods*, 285-293.
- Cole, J.J., Prairie, Y.T., Caraco, N.F., McDowell, W.H., Tranvik, L.J., Striegl, R.G., Duarte, C.M., Kortelainen, P., Downing, J.A., Middelburg, J.J. and Melack, J., 2007. Plumbing the global carbon cycle: integrating inland waters into the terrestrial carbon budget. *Ecosystems*, 10(1), pp.172-185.
- Crawford, J.T., Lottig, N.R., Stanley, E.H., Walker, J.F., Hanson, P.C., Finlay, J.C., Striegl, R.G., 2014. CO₂ and CH₄ emissions from streams in a lake-rich landscape: Patterns, controls, and regional significance. *Global Biogeochemical Cycles*, 28(3), pp.197-210.
- Crawford, J.T., Striegl, R.G., Wickland, K.P., Dornblaser, M.M., Stanley, E.H., 2013. Emissions of carbon dioxide and methane from a headwater stream network of interior Alaska. *Journal of Geophysical Research: Biogeosciences*, 118(2), pp.482-494.
- Deirmendjian, L., Abril, G., 2018. Carbon dioxide degassing at the groundwater-stream-atmosphere interface: isotopic equilibration and hydrological mass balance in a sandy watershed. *Journal of Hydrology*, 558, pp.129-143.

- Deirmendjian, L., Loustau, D., Augusto, L., Lafont, S., Chipeaux, C., Poirier, D. and Abril, G., 2018. Hydro-ecological controls on dissolved carbon dynamics in groundwater and export to streams in a temperate pine forest. *Biogeosciences*, 15(2), pp.669-691.
- Demars, B.O.L., Manson, J.R., 2013. Temperature dependence of stream aeration coefficients and the effect of water turbulence: A critical review. *Water research*, 47(1), pp.1-15.
- Dinsmore, K.J., Wallin, M.B., Johnson, M.S., Billett, M.F., Bishop, K., Pumpanen, J., Ojala, A., 2013. Contrasting CO₂ concentration discharge dynamics in headwater streams: A multi-catchment comparison. *Journal of Geophysical Research: Biogeosciences*, 118(2), pp.445-461.
- Doctor, D.H., Kendall, C., Sebestyen, S.D., Shanley, J.B., Ohte, N., Boyer, E.W., 2008. Carbon isotope fractionation of dissolved inorganic carbon (DIC) due to outgassing of carbon dioxide from a headwater stream. *Hydrological Processes: An International Journal*, 22(14), pp.2410-2423.
- Dodds, W. K. 2021. ASD02 Stream discharge measured at the flumes on watershed N04D at Konza Prairie . Environmental Data Initiative. <http://dx.doi.org/10.6073/pasta/14bad446298b9892f27ab9fc1b1dfd55>
- Gómez-Gener, L., Obrador, B., Marcé, R., Acuña, V., Catalán, N., Casas-Ruiz, J.P., Sabater, S., Muñoz, I., von Schiller, D., 2016. When water vanishes: magnitude and regulation of carbon dioxide emissions from dry temporary streams. *Ecosystems*, 19(4), pp.710-723.
- Gómez-Gener, L., Obrador, B., von Schiller, D., Marcé, R., Casas-Ruiz, J.P., Proia, L., Acuña, V., Catalán, N., Muñoz, I., Koschorreck, M., 2015. Hot spots for carbon emissions from Mediterranean fluvial networks during summer drought. *Biogeochemistry*, 125(3), pp.409-426.
- Hayden, B. P., 1998. Regional climate and the distribution of tallgrass prairie. In *Grassland Dynamics Long-Term Ecological Research in Tallgrass Prairie*. New York, NY: Oxford University Press, 1998. 19-34.
- Hélie, J.F., Hillaire-Marcel, C., Rondeau, B., 2002. Seasonal changes in the sources and fluxes of dissolved inorganic carbon through the St. Lawrence River—isotopic and chemical constraint. *Chemical Geology*, 186(1-2), pp.117-138.
- Hendry, M.J., Lawrence, J.R., Zanyk, B.N., Kirkland, R., 1993. Microbial production of CO₂ in unsaturated geologic media in a

- mesoscale model. *Water Resources Research*, 29(4), pp.973-984.
- Hope, D., Palmer, S.M., Billett, M.F., Dawson, J.J., 2001. Carbon dioxide and methane evasion from a temperate peatland stream. *Limnology and Oceanography*, 46(4), pp.847-857.
- Hotchkiss, E.R., Hall Jr, R.O., Sponseller, R.A., Butman, D., Klaminder, J., Laudon, H., Rosvall, M., Karlsson, J.J.N.G., 2015. Sources of and processes controlling CO₂ emissions change with the size of streams and rivers. *Nature Geoscience*, 8(9), pp.696-699.
- Johnson, M.S., Lehmann, J., Riha, S.J., Krusche, A.V., Richey, J.E., Ometto, J.P.H., Couto, E.G., 2008. CO₂ efflux from Amazonian headwater streams represents a significant fate for deep soil respiration. *Geophysical Research Letters*, 35(17).
- Jonsson, A., Algesten, G., Bergström, A.-K., Bishop, K., Sobek, S., Tranvik, L.j., Jansson, M., 2007. Integrating aquatic carbon fluxes in a boreal catchment carbon budget. *Journal of Hydrology* 334.1-2, pp. 141-50.
- Karim, A., Veizer, J., 2000. Weathering processes in the Indus River Basin: implications from riverine carbon, sulfur, oxygen, and strontium isotopes. *Chemical Geology*, 170(1-4), pp.153-177.
- Karlsson, J., Serikova, S., Vorobyev, S.N., Rocher-Ros, G., Denfeld, B., Pokrovsky, O.S., 2021. Carbon emission from Western Siberian inland waters. *Nature communications*, 12(1), pp.1-8.
- Kessler, T.J., Harvey, C.F., 2001. The global flux of carbon dioxide into groundwater. *Geophysical research letters*, 28(2), pp.279-282.
- Kuzyakov, Y., Domanski, G., 2000. Carbon input by plants into the soil. Review. *Journal of Plant Nutrition and Soil Science*, 163(4), pp.421-431.
- Luo, J., Li, S., Ni, M., Zhang, J., 2019. Large spatiotemporal shifts of CO₂ partial pressure and CO₂ degassing in a monsoonal headwater stream. *Journal of Hydrology*, 579, p.124135.
- MacIntyre, S., Wanninkhof, R., Chanton, J., 1995, Trace gas exchange across the air-water interface in freshwater and coastal marine environments, In: Matson RA & Harris RC (eds) *Biogenic trace gases: Measuring emissions from soil and water*, In: Lawton JH & Likens GE (series eds.) *Methods in Ecology*, pp 52-97. Blackwell Science, Oxford p. 52-97.
- Macpherson, G.L., 1996. Hydrogeology of thin-bedded limestones - the Konza Prairie LTER site, northeastern Kansas. *Journal of Hydrology*, 186(1-4), 191-229.

- Macpherson, G.L., 2009. CO₂ distribution in groundwater and the impact of groundwater extraction on the global C cycle. *Chemical Geology*, 264(1-4), pp.328-336.
- Macpherson, G.L., Sophocleous, M., 2004. Fast ground-water mixing and basal recharge in an unconfined, alluvial aquifer, Konza LTER Site, Northeastern Kansas. *Journal of Hydrology*, 286(1-4), pp.271-299.
- Macpherson, G.L., Sullivan, P.L., 2019. Watershed-scale chemical weathering in a merokarst terrain, northeastern Kansas, USA. *Chemical Geology*, 527, p.118988.
- Macpherson, G.L., Roberts, J.A., Blair, J.M., Townsend, M.A., Fowle, D.A., Beisner, K.R., 2008. Increasing shallow groundwater CO₂ and limestone weathering, Konza Prairie, USA. *Geochimica et Cosmochimica Acta*, 72(23), pp.5581-5599.
- Macpherson, G. L. 2020. AGW03 Konza Prairie Long-term high frequency groundwater level and temperature from wells on N04d. Environmental Data Initiative. <http://dx.doi.org/10.6073/pasta/20b8bf4b57cabf7c8fbd7bd99f09b43e>.
- Marx, A., Dusek, J., Jankovec, J., Sanda, M., Vogel, T., Van Geldern, R., Hartmann, J., Barth, J.A.C., 2017. A review of CO₂ and associated carbon dynamics in headwater streams: A global perspective. *Reviews of Geophysics*, 55(2), pp.560-585.
- Mayorga, E., Aufdenkampe, A.K., Masiello, C.A., Krusche, A.V., Hedges, J.I., Quay, P.D., Richey, J.E., Brown, T.A., 2005. Young organic matter as a source of carbon dioxide outgassing from Amazonian rivers. *Nature*, 436(7050), pp.538-541.
- Meals, D. W., Dressing, S. A., 2008. Surface water flow measurement for water quality monitoring. Retrieved from EPA Tech Notes: https://www.epa.gov/sites/production/files/2016-05/documents/tech_notes_3_dec2013_surface_flow.pdf
- Monger, H.C., Kraimer, R.A., Khresat, S.E., Cole, D.R., Wang, X. and Wang, J., 2015. Sequestration of inorganic carbon in soil and groundwater. *Geology*, 43(5), pp.375-378.
- Müller, D., Warneke, T., Rixen, T., Müller, M., Jamahari, S., Denis, N., Mujahid, A., Notholt, J., 2015. Lateral carbon fluxes and CO₂ outgassing from a tropical peat-draining river. *Biogeosciences*, 12(20), pp.5967-5979.
- Nadeau, T.L., Rains, M.C., 2007. Hydrological connectivity between headwater streams and downstream waters: how science can inform policy 1. *JAWRA Journal of the American Water Resources Association*, 43(1), pp.118-133.

- Nippert, J., 2017. AWE01 Meteorological data from the konza prairie headquarters weather station. Konza Prairie Long Term Ecological Research (LTER) Program. doi:10.6073/pasta/0e0c648068f3f2755e0b500062a4f7e9
- Nippert, J.B. and Knapp, A.K., 2007. Soil water partitioning contributes to species coexistence in tallgrass prairie. *Oikos*, 116(6), pp.1017-1029.
- Norwood, B. N., 2020. Flux and stable isotope fractionation of CO₂ in a headwater stream. Unpublished M.S. thesis, University of Kansas, 92 pp.
- NRCS (National Resources Conservation Service), 2006, Soils in Riley and Geary Counties, Kansas. NRCS, accessed online 11/2/2006, 11:15 am.
- Pomes, M. L., 1995. A study of the aquatic humic substances and hydrogeology in a prairie watershed—Use of humic material as a tracer of recharge through soils. Ph.D. dissertation, University of Kansas, 296 pp.
- Ranson, M.D., Rice, C.W., Todd, T.C., Wehmueller, W.A., 1998. Soils and soil biota. In: Knapp, A.K., Briggs, J.M., Hartnett, D.C., Collins, S.L. (Eds.), *Grassland Dynamics—Long-term Ecological Research in Tallgrass Prairie*. Oxford University Press, New York, pp. 48–68.
- Rawitch, M., Macpherson, G. L., Brookfield, A., 2019. Exploring methods of measuring CO₂ degassing in headwater streams. *Sustainable Water Resources Management* 5.4: 1765-779.
- Rawitch, M.J., Macpherson, G.L., Brookfield, A.E., 2021. The validity of floating chambers in quantifying CO₂ flux from headwater streams. *Journal of Water and Climate Change*, 12(2), pp.453-468; doi: 10.2166/wcc.2020.199.
- Reitz, O., Graf, A., Schmidt, M., Ketzler, G., Leuchner, M., 2021. Upscaling net ecosystem exchange over heterogeneous landscapes with machine learning. *Journal of Geophysical Research: Biogeosciences*, 126(2), p.e2020JG005814.
- Riveros-Iregui, D.A., McGlynn, B.L., 2009. Landscape structure control on soil CO₂ efflux variability in complex terrain: Scaling from point observations to watershed scale fluxes. *Journal of Geophysical Research: Biogeosciences*, 114(G2).
- Saccardi, B., Winnick, M., 2021. Improving predictions of stream CO₂ concentrations and fluxes using a stream network model: a Case study in the East River Watershed, CO, USA. *Global Biogeochemical Cycles*, 35(12), p.e2021GB006972.

- Sand-Jensen, K., Staehr, P.A., 2012. CO₂ dynamics along Danish lowland streams: water–air gradients, piston velocities and evasion rates. *Biogeochemistry*, 111(1), pp.615-628.
- Schlesinger, W.H. and Lichter, J., 2001. Limited carbon storage in soil and litter of experimental forest plots under increased atmospheric CO₂. *Nature*, 411(6836), pp.466-469.
- Schlesinger, W.H., Melack, J.M., 1981. Transport of organic carbon in the world's rivers. *Tellus*, 33(2), pp.172-187.
- Striegl, R.G., Dornblaser, M.M., McDonald, C.P., Rover, J.R., Stets, E.G., 2012. Carbon dioxide and methane emissions from the Yukon River system. *Global Biogeochemical Cycles*, 26(4).
- Sullivan, P.L., Zhang, C., Behm, M., Zhang, F., Macpherson, G.L., 2020. Toward a new conceptual model for groundwater flow in merokarst systems: Insights from multiple geophysical approaches. *Hydrological Processes*, 34(24), pp.4697-4711. DOI: 10.1002/hyp.13898.
- Taylor, C.B. and Fox, V.J., 1996. An isotopic study of dissolved inorganic carbon in the catchment of the Waimakariri River and deep ground water of the North Canterbury Plains, New Zealand. *Journal of hydrology*, 186(1-4), pp.161-190.
- Tsy-pin, M., Macpherson, G.L., 2012. The effect of precipitation events on inorganic carbon in soil and shallow groundwater, Konza Prairie LTER Site, NE Kansas, USA. *Applied Geochemistry*, 27(12), pp.2356-2369; doi:10/1016/j.apgeochem.2012.07.008.
- Twiss, P. C., 1988. Beattie Limestone (Lower Permian) of Eastern Kansas. *Centennial Field Guide Volume 4: South-Central Section of the Geological Society of America*: 35-41.
- USGS, 2016. How Streamflow Is Measured: The Discharge Measurement. *How Streamflow Is Measured*. N.p., n.d. Web. Jan. 2016.
- Veach, A.M., Dodds, W.K., Skibbe, A., 2014. Fire and grazing influences on rates of riparian woody plant expansion along grassland streams. *PloS one*, 9(9), p.e106922.
- Venkiteswaran, J.J., Schiff, S.L., Wallin, M.B., 2014. Large carbon dioxide fluxes from headwater boreal and sub-boreal streams. *PloS one*, 9(7), p.e101756.
- Wang, C., Guo, L., Li, Y., Wang, Z., 2012. Systematic comparison of C3 and C4 plants based on metabolic network analysis. *In BMC systems biology* (Vol. 6, No. 2, pp. 1-14). BioMed Central.
- Wanninkhof, R., 2014. Relationship between wind speed and gas exchange over the ocean revisited. *Limnology and Oceanography*:

Methods, 12(6), pp.351-362.

Warner, D.L., Guevara, M., Inamdar, S., Vargas, R., 2019. Upscaling soil-atmosphere CO₂ and CH₄ fluxes across a topographically complex forested landscape. *Agricultural and Forest Meteorology*, 264, pp.80-91.

Weary, D.J. and Doctor, D.H., 2014. *Karst in the United States: a digital map compilation and database* (p. 26). Reston, VA, USA: US Department of the Interior, US Geological Survey.

Wen H., Sullivan P. L., Macpherson G. L., Li L., 2021. Deepening roots enhance carbonate weathering by amplifying CO₂-rich recharge. *Biogeosciences* 18, p. 55-75. <https://doi.org/10.5194/bg-18-55-2021>

Winter, T.C., Harvey, J.W., Franke, O.L. and Alley, W.M., 1998. *Ground Water and Surface Water*: US Department of the Interior, US Geological Survey.

Yang, C., Telmer, K., Veizer, J., 1996. Chemical dynamics of the “St. Lawrence” riverine system: D_{H₂O}, ¹⁸O_{H₂O}, ¹³C_{DIC}, ³⁴S_{sulfate}, and dissolved ⁸⁷Sr/⁸⁶Sr. *Geochimica et Cosmochimica Acta*, 60(5), pp.851-866.

Zeller, D.E., 1968. The Stratigraphic Succession in Kansas. *Kansas Geological Survey Bulletin* 189.